Iran. J. Sci. Technol. Trans. Mech. Eng. (2016) 40:139–149
DOI 10.1007/s40997-016-0013-9

TECHNICAL NOTE

Aerodynamic Characteristics Investigation of a Passenger Train Under Crosswind

M. Rabani[1] · A. K. Faghih[1] · R. Rabani[1]

Received: 13 June 2014 / Accepted: 26 October 2015 / Published online: 11 May 2016
© Shiraz University 2016

Abstract The aim of this study is to investigate experimentally and numerically the effect of the crosswind and wagon numbers to the aerodynamic characteristics as well as fuel consumption of the locomotive Alstom AD43C and some specified passenger wagons behind it. Turbulent, incompressible, and 3D airflow has been considered for numerical simulation. Simulations are carried out for yaw angles 0°, 15°, and 30° for different airflow velocities. A total of 16 pressure tabs were employed to measure the air pressure at various points on the 1:26 scaled model of the train in the experimental investigation. Comparison between the numerical and the experimental results verifies the numerical simulation method. The results show that the variation of the longitudinal force coefficient (LFC) and side force coefficient (SFC) in the middle wagons (except for the first two and last two wagons) is similar. The LFC and SFC of these wagons are 0.239 and 1.251, respectively, for the Reynolds number 1.587×10^5 (airflow velocity 30 m/s) and the yaw angle 30°. However, the Reynolds number effect is insignificant. The yaw angle effect on the train fuel consumption is more important. Moreover, the fuel consumption increases by approximately 25 % from the yaw angle 0° to 30° for ten wagons at the Reynolds number 1.587×10^5.

Keywords Numerical simulation · Experimental investigation · Passenger train · Crosswind · Longitudinal force coefficient · Side force coefficient

List of symbols

A_x	Cross section of the object in the plane perpendicular to the X (m^2)
C_P	Pressure coefficient
C_x	Longitudinal force coefficient
C_z	Side force coefficient
C_μ	Model constant
F_x	Longitudinal force (N)
F_z	Side force (N)
Re	Reynolds number
V	Airflow velocity (m/s)
g	Acceleration due to gravity (m/s^2)
h	Pressure head (mm H_2O)
k	Turbulent kinetic energy
p	Mean static pressure (Pa)
u	Mean velocity (m/s)

Greek symbols

η	Scale of the model
δ	Kronecker delta
ε	Dissipation rate
ρ	Density (kg/m^3)
μ	Dynamic viscosity (Pa s)
μ_t	Turbulent dynamic viscosity (Pa s)

Subscripts

a	Air
$i, j = 1, 2, 3$	x, y, z direction, respectively
w	Water

✉ M. Rabani
mehrdad-rabani@stu.yazd.ac.ir

[1] School of Mechanical Engineering, Yazd University, Yazd, Iran

1 Introduction

One of the important parameters for train passengers' comfort is a uniform pressure distribution around the train body. Determination of the train aerodynamic behavior is required in order to optimize the performance and the stability of the passenger trains. In high train speeds, the effects of crosswind, the drag, and the momentum forces which affect the train stability are also important. When a high-speed train moves in a side wind, the effective side wind is strong even if the magnitude of the side wind velocity is low. The effective side wind is the result of the train and the side wind speeds.

The angle between the effective side wind direction and the train moving direction is called the yaw angle, as shown in Fig. 1. Normally, side wind yaw angles are below 40° owing to relatively low-speed side winds compared to the train speed. However, it is possible to find high-speed trains that are moving at the larger yaw angles, e.g., when they exit from tunnels or when a strong side wind has a strong component in the direction of the train motion.

The new generation of high-speed trains is light in weight in order to provide high acceleration and reduce the energy which is necessary to overcome gravity and friction forces. When these trains move in a strong side wind, there is a stagnation region with high pressure on the streamwise face while a region of low pressure is formed on the lee side due to the recirculation regions in the wake flow. In addition, the flow moves over the train roof at high velocity, making a region of low pressure on the upper side of the train. Due to these pressure differences, the high-speed trains experience strong aerodynamic forces and moments such as side and lift forces and a yaw moment, as shown in Fig. 2. In such conditions, the high-speed trains are at high risk of overturning or derailment.

There are many researches to determine the flow characteristics around the rigid bodies and their aerodynamic behavior (Hemidia 2006; Copley 1987; Motallebi Hasankola et al. 2012). Airflow around the trains along with the side wind has been investigated experimentally by several researchers (Chiu and Squire 1992; Hoppmann et al. 2002; Baker 2003; Suzuki et al. 2003). The primary interest in these investigations was the measurement of some integral parameters such as drag, lift, and side force coefficients

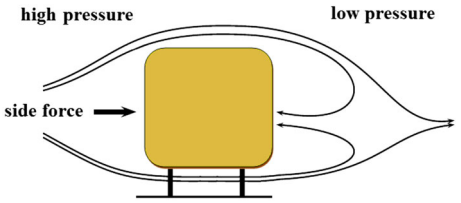

Fig. 2 Aerodynamic forces and moments due to side wind

together. Some other researches numerically investigate the airflow distribution around the train with crosswind (Baker et al. 2004; Durst et al. 2000; Diedrichs 2003). Numerical study could be an alternative owing to the right Reynolds number value that can be considered in the calculations and the high quantity of data delivered, which is useful to understand the flow structure and the pressure fields on the envelope of the train. Furthermore, the investigation of the airflow around the high-speed train under the crosswinds by Sanquer et al. (2004), Baker (2010), and Muld et al. (2012) has been performed. Aerodynamics of open cargo railway trains has been investigated by Churkov (2007), Astakhov (1966) and Hoerner (1965) as well. The effect of freight wagon number on the longitudinal and side forces has been also studied by Golovanevskiy et al. (2012). The results of their investigation revealed that the optimal model configuration consists of six freight wagons with two streamlined bodies at the beginning and the end of the train. Jalili et al. (2011) in an experimental work investigated the effect of the various sizes of iron ore and the type of the freight wagons on the iron ore waste when the airflow passes over the train. The results indicated that the wagons of type 1 and 3, respectively, have the least amount of waste for the small and large scale of iron ore. Holmes et al. (2000) conducted a series of numerical simulations to characterize the aerodynamic loads on a container consistently passed by a high-speed train. Vasovic et al. (2011) presented numerically the stress and the stability of aerodynamic brakes for a high-speed train.

In all previous studies, the main aim was the investigation of train stability in the presence of cross wind. The determination of the high- and low-pressure areas for different train speeds, wagon numbers, and yaw angles plays an important role in the improvement of transportation quality and the reduction in train fuel consumption.

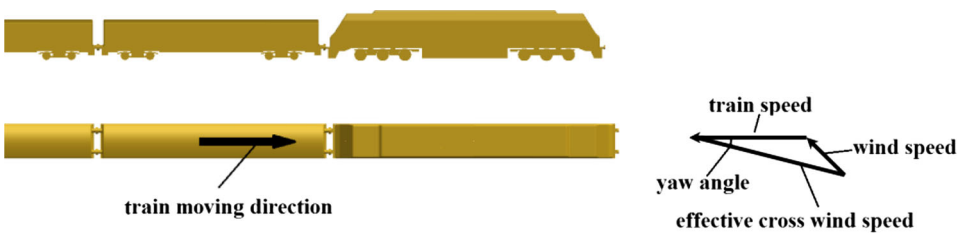

Fig. 1 Effective side wind

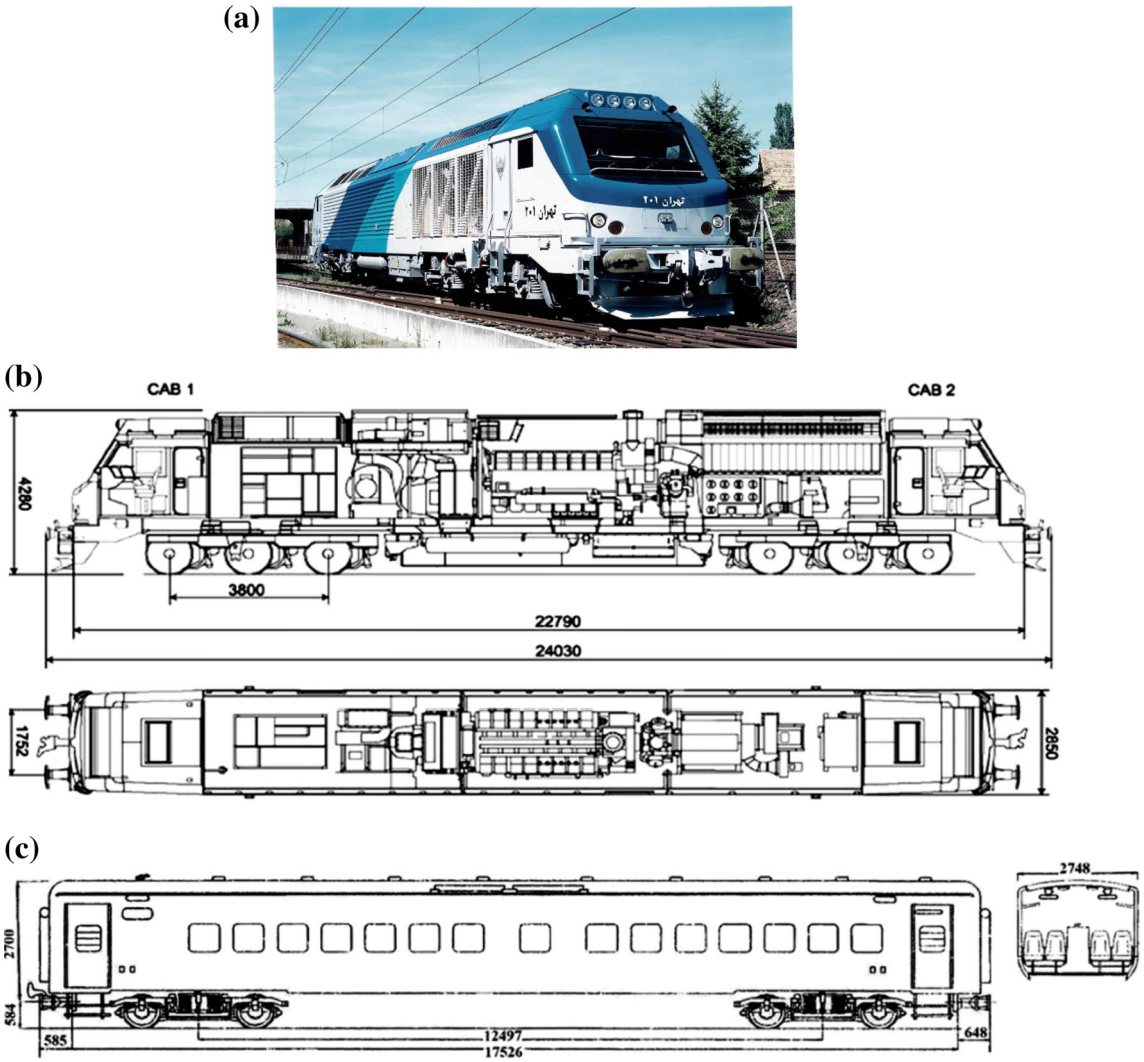

Fig. 3 **a** View of locomotive Alstom AD43C, **b** the actual dimensions of the locomotive, **c** the actual dimensions of the passenger wagon. *Note* Unit of dimensions is millimeter

Therefore, in the present study, the pressure coefficient of specific points on the locomotive (Alstom AD43C) and a passenger wagon behind it have been numerically and experimentally studied for yaw angle 0°. Air pressure distribution and longitudinal and side forces, as well as the fuel consumption of train, have been numerically studied for different airflow velocities, wagon numbers, and yaw angles.

2 Experimental Investigation

In order to obtain a better understanding of the airflow behavior passing through the passenger train, an experimental investigation has been performed in Yazd University wind tunnel. The wind tunnel is the Eiffel-type, low-speed tunnel which is able to produce a maximum wind velocity of 30 m/s, and turbulence intensity is less than 0.13 %. It has a closed test section with cross-sectional area of 457 × 457 mm and length of 1200 mm. The considered geometry of the real train consists of the locomotive Alstom AD43C and a specific passenger wagon of Iran railways, which is shown in Fig. 3. A scaled model of the locomotive along with the wagon behind it has been made. The model scale is limited by the ratio of the frontal area of the model to the cross-sectional area of the wind tunnel (blockage ratio). Due to the fact that there were some experimental limitations for measuring the air pressure on the train model, the maximum blockage ratio was considered to be 10 %. However, this ensures that potential edge effects during the wind tunnel testing are almost minimized.

The proper scale in this study is calculated using Eq. (1). In this equation, η is the scale of the model. Figure 4 shows

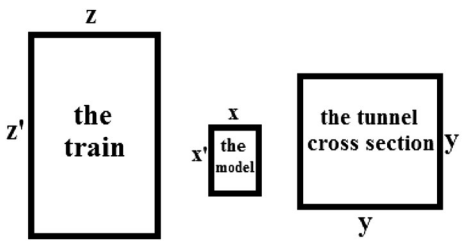

Fig. 4 A schematic of the frontal area of the train and the model as well as the wind tunnel cross section

a schematic of the frontal area of the train and the model as well as the wind tunnel cross section.

$$y = 457\ \text{mm},\ z = 285\ \text{mm},\ z' = 428\ \text{mm}$$
$$\frac{xx'}{y^2} = 0.1, \alpha = \frac{zz'}{xx'} = \frac{zz'}{0.1y^2} = \frac{10zz'}{y^2} = 584.058 \quad (1)$$
$$\eta = \sqrt{\alpha} = \frac{z'}{x'} = \frac{z}{x} = 24.167$$

Regarding the scale of the model (η) which is determined in Eq. (1), the model scale can be adopted greater than η, which is selected 26 in this study.

According to the real dimensions of the locomotive and the wagon (Fig. 3b, c) and the model scale 1:26, the train model is designed and made. It should be noted that in the train model, some simplifications have been implemented. The aim of these simplifications was to facilitate the modeling of train body for numerical simulation of airflow around the train model.

Figure 5 shows the final assembled model of the locomotive and wagon (a), and the model fixation in the test section of the wind tunnel (b). Regarding the fact that the airflow velocity is up to 30 m/s, the model should be firmly fixed inside the test section. Therefore, special screws are built for fixing the model in the wind tunnel. These screws are used at the end of the model, where it has no significant effect on the upstream airflow pattern. Two thin wires have been used to fix the train nose to the test section windows.

Some water manometer tubes (pressure tabs) are used on the different points of the train body. The number of tubes is 17 including 16 tubes for different points of the train body shown in Fig. 6, and a tube placed in front of the model with appropriate distance in order to measure the static head of oncoming airflow (h_∞). All pressure tubes are collected and exited thorough a pressure bank from behind the wagon model which is shown in Fig. 5b. The pressure coefficient is determined in Eq. (2).

$$C_p = \frac{\rho_w g(h - h_\infty)}{1/2\rho_a V^2} \quad (2)$$

3 Numerical Simulation

In this study, a 3D model of airflow over a locomotive and some passenger wagons behind it has been numerically simulated. The effect of the number of wagons, Reynolds number (airflow velocity), and the yaw angle of crosswind

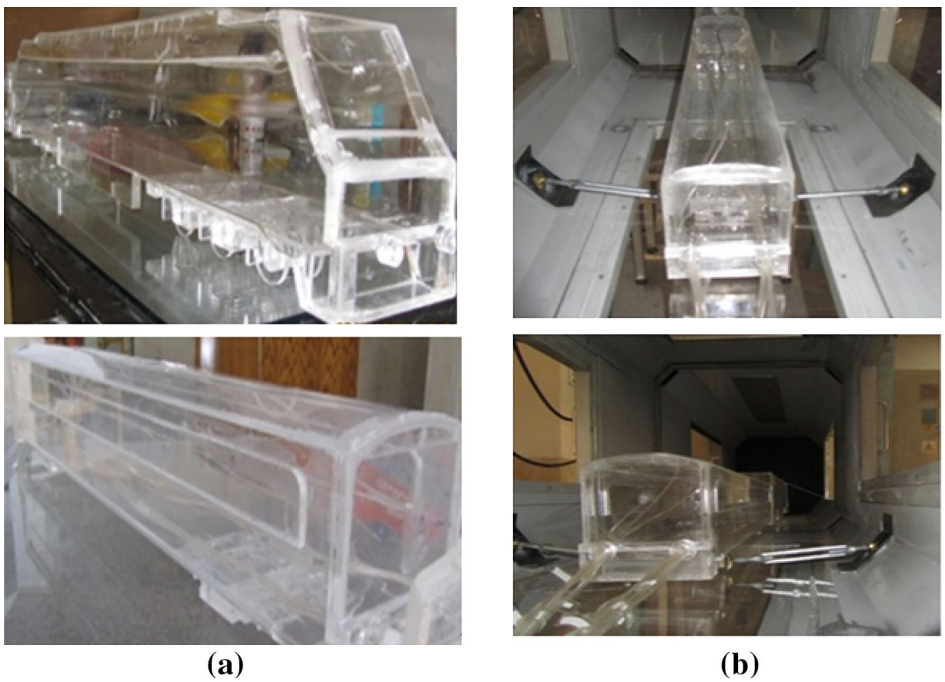

Fig. 5 **a** Final assembled model of the locomotive and wagon, **b** the model fixation in the wind tunnel test section

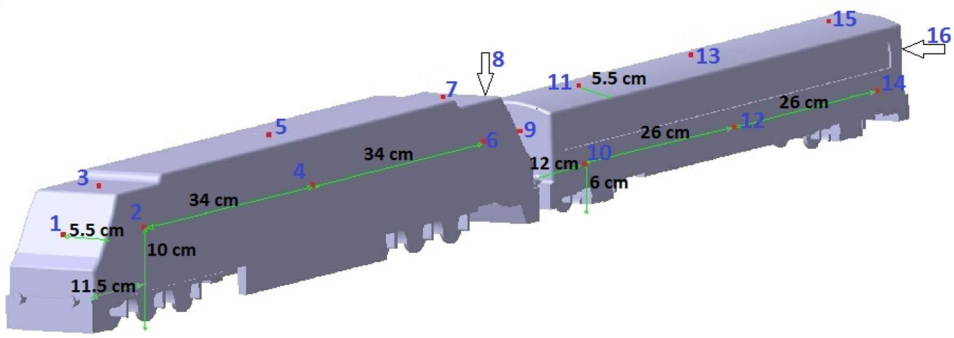

Fig. 6 Position of all pressure tabs on the train model

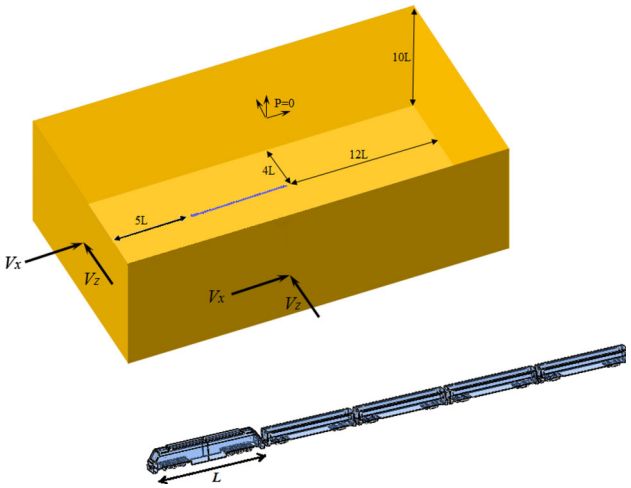

Fig. 7 A view of the boundary conditions and the size of the computational domain

on the pressure distribution, longitudinal force coefficient (LFC), and side force coefficient (SFC) has been investigated.

3.1 Geometry and Boundary Conditions

The following boundary conditions are determined with regard to the work of Golovanevskiy et al. (2012) (Fig. 7):

- At the inlets, velocities V_x and V_z along the X and Z axes were adopted, with zero velocity V_y along the Y axes;
- At the outlets, static pressure P was set at $P = 0$;
- No-slip condition at the surfaces of the train body and the ground.

The dimensions of a computational domain which are shown in Fig. 7 were selected so that the disturbances emerging in aerodynamic trail of a wagon disappeared.

3.2 Governing Equations

The aerodynamic of train system is solved by a three-dimensional, steady, viscous, turbulent, incompressible and Newtonian flow model. The governing equations are the continuity equation and the Navier–Stokes equation which describe the physical principles of conservation of mass and momentum, respectively. They can be written in Cartesian tensor as:

$$\frac{\partial u_i}{\partial x_i} = 0 \tag{3}$$

$$\rho\left(u_j \frac{\partial u_i}{\partial x_j}\right) = -\frac{\partial p}{\partial x_i} + \frac{\partial}{\partial x_j}\left(\mu \frac{\partial u_i}{\partial x_j} - \rho\left(\overline{u_i' u_j'}\right)\right) \tag{4}$$

In Eq. (4), the terms $-\rho\left(\overline{u_i' u_j'}\right)$ are the time-averaged Reynolds stresses, representing the turbulent momentum fluxes. Based on the Boussinesq hypothesis, the Reynolds stresses are related to the mean velocity gradients and can be written in Eq. (5) as follows:

$$-\rho\left(\overline{u_i' u_j'}\right) = \mu_t\left(\frac{\partial u_i}{\partial x_j} + \frac{\partial u_j}{\partial x_i}\right) - \frac{2}{3}\rho k \delta_{ij} \tag{5}$$

where μ_t and k are defined as:

$$k = \frac{1}{2}\left(\overline{u_i' u_j'}\right) \tag{6}$$

$$\mu_t = \rho C_\mu \frac{k^2}{\varepsilon} \tag{7}$$

where ε is defined as:

$$\varepsilon = \frac{\mu}{\rho}\overline{\left(\frac{\partial u_i'}{\partial x_j}\right)\left(\frac{\partial u_i'}{\partial x_j}\right)} \tag{8}$$

Commercially available software (ANSYS/FLUENT 14) is employed in this numerical investigation. As compared with the standard methods of analysis, the *k-εRNG* model for turbulence simulation is adopted in this study due to its

higher accuracy. Second-order upwind method is used to make the related equations discrete. The solution method is a control volume, using incompressible model. Pressure and velocity dependency method is SIMPLE (Wilcox 1994).

3.3 Aerodynamic Coefficients and Reynolds Number

When the moving train faces the crosswind, aerodynamic forces such as the longitudinal (F_x) and the cross (F_z) forces play an important role in train stability. To compare the effect of these forces on the aerodynamic performance, the aerodynamic coefficients are used. In this study, the aerodynamic coefficients are defined as follows:

$$C_x = \frac{F_x}{\frac{1}{2}\rho V^2 A_x} \tag{9}$$

$$C_z = \frac{F_z}{\frac{1}{2}\rho V^2 A_x} \tag{10}$$

In Eqs. (9) and (10), F is the summation of frictional and pressure forces.

Determination of the Reynolds number requires knowledge of the oncoming airflow velocity and the characteristic dimension of the model. In this study, the characteristic dimension was taken as the length of the locomotive model $L = 920$ mm. Therefore, the Reynolds number is determined as:

$$Re = \frac{VL}{v} \tag{11}$$

where V, L, and v are the airflow velocity, the characteristic dimension of the body, and the kinematic viscosity of air, respectively. Table 1 represents the calculated Reynolds number values for 1:26 scale train model and different airflow velocities.

Regarding the independency of aerodynamic characteristics of the passenger train from Reynolds number, it was thoroughly discussed in the work of Golovanevskiy et al. (2012). They note that in the case of frontal air drag of a long cargo railway train, a railcar can be considered a quasi-square prism with fineness ratio f (i.e., width-to-depth ratio) of $f \leq 1$, which satisfies the non-dependency of Reynolds number. Accordingly, in the present study, the locomotive can be considered as a quasi-square prism. Afterward, using the 1:26 scale model dimensions, the calculation of fineness ratio of the locomotive (ratio of width to the length of the locomotive) results in $f \approx 0.13$, and therefore, this satisfies the condition $f \leq 1$ of non-dependency of Reynolds number.

Table 1 Reynolds number values in different airflow velocity for 1:26 scale train model

Airflow velocity	$Re \times 10^5$
15	0.794
20	1.058
25	1.322
30	1.587

3.4 Mesh Generation

In order to reticulate the computational domain and select the best grid number considering the results accuracy at the minimum CPU time, six different grid numbers are considered and the variation of the total LFC in yaw angle 0° is illustrated in Fig. 8. As it is evident in this figure, the variation of the total LFC for number of grids from 3,806,758 to 5,123,400 is less than 1 %. So, the grid number of 3,806,758 is considered.

Figure 9 shows a view of the grid density around the train. To encompass small elements likely to emerge in the partition zone, the adaptive mesh was designed to be

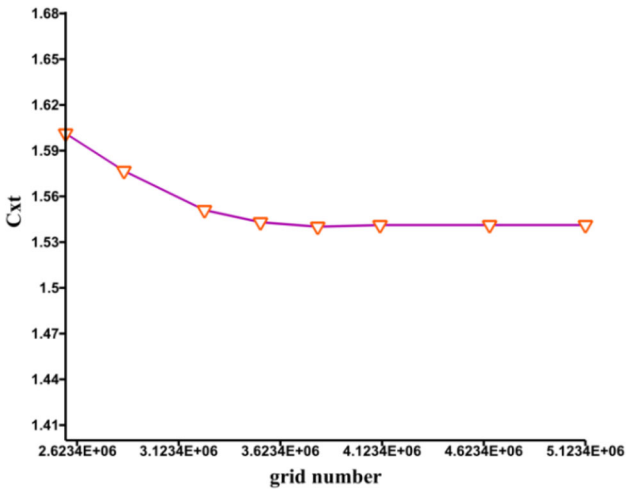

Fig. 8 Variation of the total LFC in different grid numbers for the locomotive with ten wagons in $Re = 1.587 \times 10^5$ (the airflow velocity 30 m/s) and yaw angle 0°

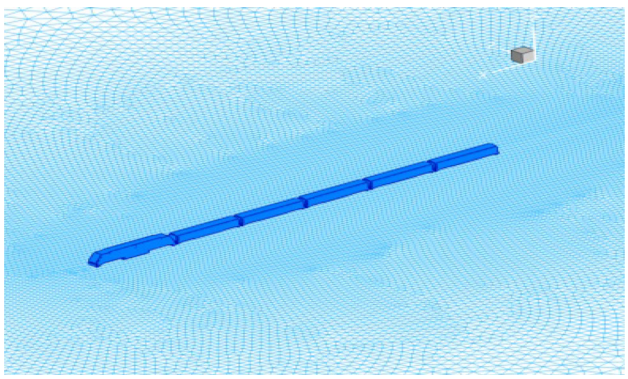

Fig. 9 Model train with adaptive mesh

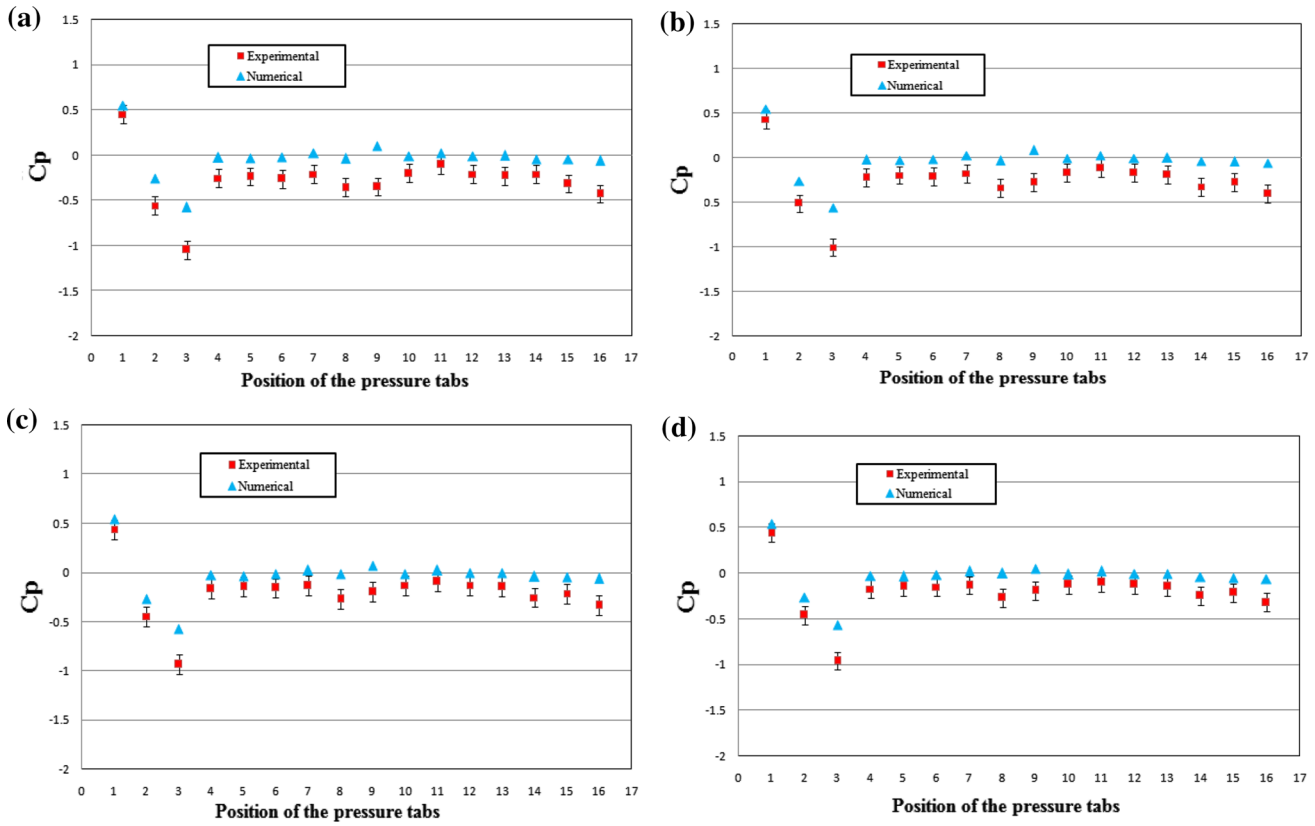

Fig. 10 Pressure coefficients for some specified points on the train body for Reynolds number **a** $Re = 0.794 \times 10^5$, **b** $Re = 1.058 \times 10^5$, **c** $Re = 1.322 \times 10^5$ and **d** $Re = 1.587 \times 10^5$

sufficiently dense to take into consideration the participation of these elements in detached flows (i.e., when vortexes separate from their edges). Thus, in the vicinity of the locomotive and wagons, the mesh has the highest density while becoming less dense with the increasing distance from the train (Plewa et al. 2005).

4 Results and Discussion

For validation of numerical simulation results, the pressure coefficients obtained from the numerical and experimental investigation have been compared for different Reynolds numbers at the yaw angle 0° (Fig. 10). It should be noted that the uncertainty analysis has been performed for experimental results using the Adams method (1975). The maximum pressure coefficient error is ±8 % at the Reynolds number 0.794×10^5 (the airflow velocity 15 m/s) which is considered in the experimental results (Fig. 10). The maximum and minimum pressure coefficients have been obtained, respectively, for the points 1 and 3 at different Reynolds numbers. It seems reasonable, because the point 1 is placed in the vicinity of the locomotive stagnation point and the point 3 is located in the flow separation region at the beginning of the locomotive's roof. These values are obtained by about 0.45 and −0.95 through the experimental investigation and 0.54 and −0.61 through the numerical simulation results at the Reynolds number 1.587×10^5 (case d). The pressure coefficient of the points located on the side surface of the locomotive body (4 and 6) and that of the wagon body (10, 12 and 14) is almost identical because the train is not exposed to the side wind. Neither the experimental nor the numerical results are exact, so a difference between these results can be expected. Nevertheless, due to separation which happens at some points, especially at the point 3, this difference is more pronounced. It can be explained by the fact that at these points, it is explainable the vortex shedding phenomenon occurs, which is inherently transient.

In Fig. 11, the variation of the total LFC (Cx_t) with the number of passenger wagons is demonstrated for three yaw angles (α) and four different Reynolds numbers. It should be noted that in all cases, the presence of locomotive in front of all passenger wagons has been considered. To calculate Cx_t, the frictional and pressure forces for the configuration of the locomotive along with all passenger wagons behind it have been considered. The results indicate that with an increase in the number of passenger

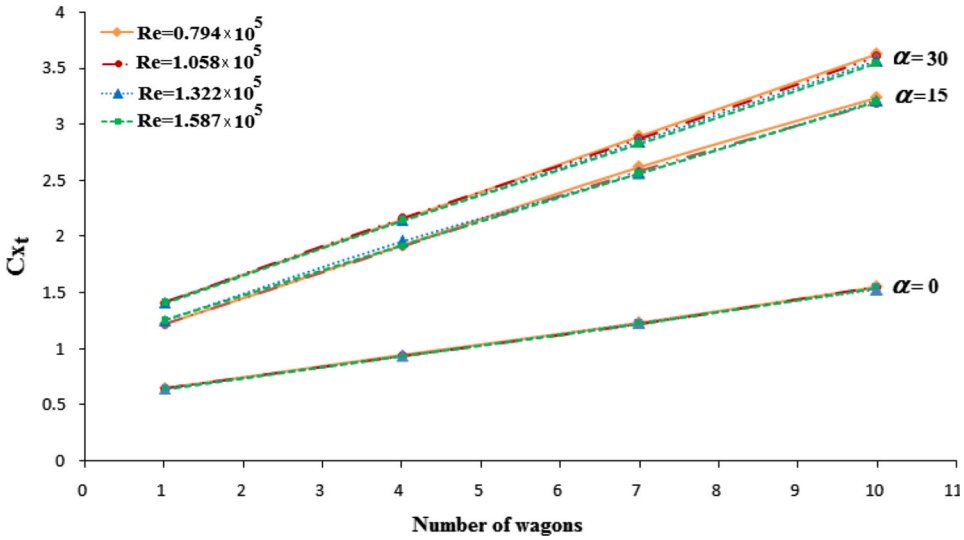

Fig. 11 Variation of the total LFC (Cx_t) versus the number of passenger wagons for three yaw angles (α) and four different Reynolds numbers

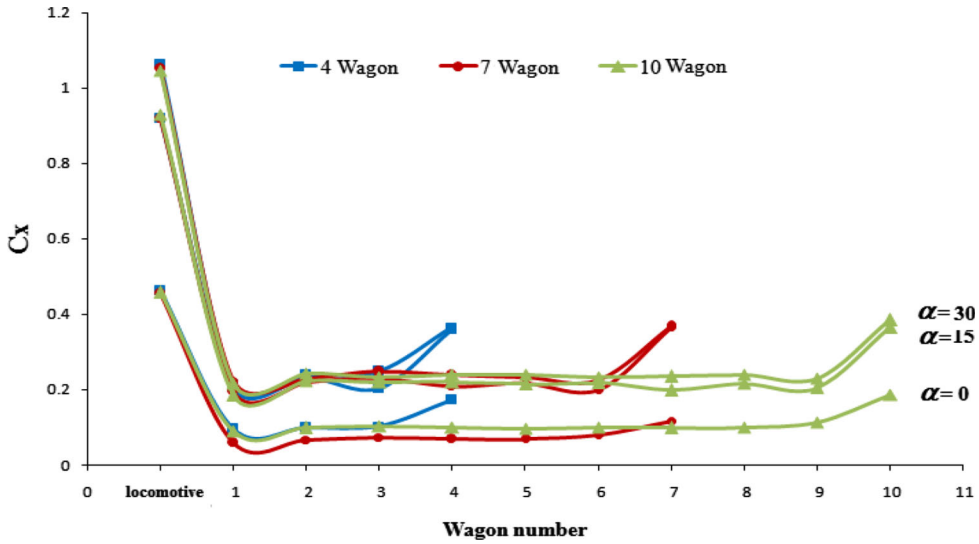

Fig. 12 Variation of the LFC versus the number of wagons for Reynolds number 1.587×10^5 for different yaw angles

wagons, the resistance to the airflow increases, which in turn causes the Cx_t to increase. Comparison of Cx_t for the yaw angle 0° and 15° reveals that the side wind effects on the longitudinal forces are more pronounced. With an increase in the yaw angle, the Cx_t increases because the flow separation region on the lee side enlarges, generating a recirculation and low-pressure region in this area. A pressure decrease in these areas not only increases the side force on the passenger wagons, but also affects the pattern of the airflow around the locomotive and the passenger wagons which in turn causes the Cx_t to increase. The maximum Cx_t for the configuration of locomotive along with ten passenger wagons is almost 1.55 and 3.565 at yaw angle 0° and 30°, respectively.

The effect of Reynolds number on the Cx_t is trivial. Consequently, the variation of Cx and Cz for each wagon has been presented only for the Reynolds number 1.587×10^5 (Figs. 12, 13). The locomotive has greater LFC and SFC compared with other passenger wagons due to its exposure to the free airflow. The maximum LFC and SFC are, respectively, equal to 1.046 and 2.612 for the yaw angle 30°. In all three cases (four, seven, and ten passenger wagons), the variation of the LFC and SFC in the middle wagons (except for the first two and last two wagons) is similar. Thus, the average value of the aerodynamic characteristics of these wagons can be considered as the aerodynamic characteristic of this specific passenger wagon when it is placed in the middle of the train. It should be noted that this result was also reported by Golovanevskiy et al. (2012) for long cargo railway trains. The average LFC and SFC for Reynolds number 1.587×10^5 are 0.1 and 0.004 at yaw angle 0°; 0.221 and 0.416 at yaw angle

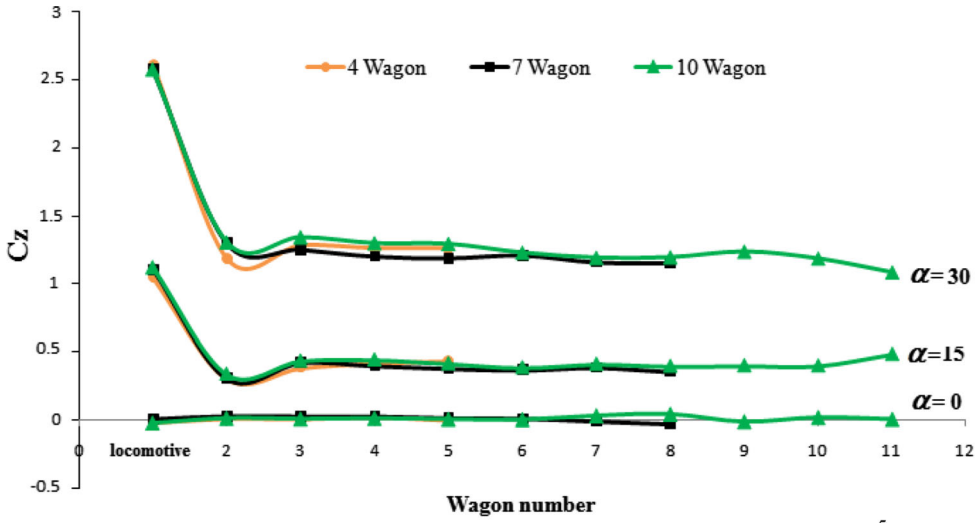

Fig. 13 Variation of the SFC versus the number of wagons for Reynolds number 1.587×10^5 for different yaw angles

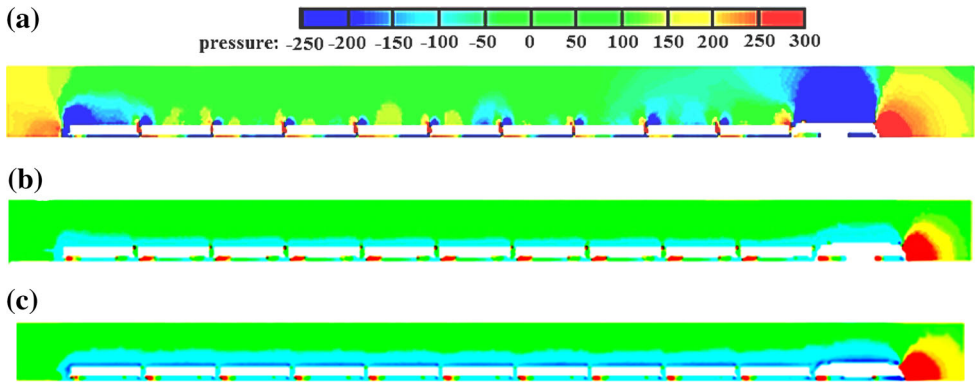

Fig. 14 Pressure distribution on the passenger train in the symmetry plane (the train is moving from left to right) at **a** $\alpha = 0°$, **b** $\alpha = 15°$ and **c** $\alpha = 30°$ for Reynolds number 1.587×10^5

15°; and 0.239 and 1.251 at yaw angle 30°, respectively. Due to the airflow separation at the back of the last wagon, the LFC increases; however, this separation has not affected the SFC of this wagon compared with other middle wagons.

In Fig. 14, the pressure distribution in the symmetry plane of the train for Reynolds number 1.587×10^5 at different yaw angles is shown. The results demonstrate that:

- With an increase in the yaw angle, the pressure distribution around the train is more uniform.
- At the yaw angle 0°, low air pressure zone behind the last wagon influences one wagon in front of the last wagon and causes the LFC of this wagon to increase by approximately 10 % compared with its average for the other middle wagons. The same result was also reported by Golovanevskiy et al. (2012) for the air resistance of the cars of an open cargo railway.
- With an increase in the yaw angle, from case (a) to (b), the low air pressure zone behind the last wagon is expanded and causes the ratio of the last wagon LFC to the LFC of the wagon located in front of it to increase by approximately 5 %. The increase in yaw angle from case (b) to (c) does not affect this ratio due to the similar pattern of the air pressure distribution around the last wagon for the two cases.

Obviously, the aerodynamic forces effect on the train fuel consumption is more important. Therefore, in this study, the ratio of the total longitudinal force to the traction force has been investigated for different airflow velocities, the number of wagons, and various yaw angles as presented in Fig. 15. The locomotive real traction force is obtained from the Fig. 16. With an increase in the Reynolds number, the yaw angle, and the number of wagons, the ratio of the total longitudinal force to the locomotive traction force increases due to the increase in the resistance of airflow. Comparison of case (a) and (b) indicates that the deviation of airflow direction from yaw angle 0° has a significant effect on the train fuel consumption. For the configuration of the locomotive along with ten wagons behind it, this ratio has been obtained by about 0.112 and 0.232 at the yaw angles 0° and 15°, respectively, for the Reynolds

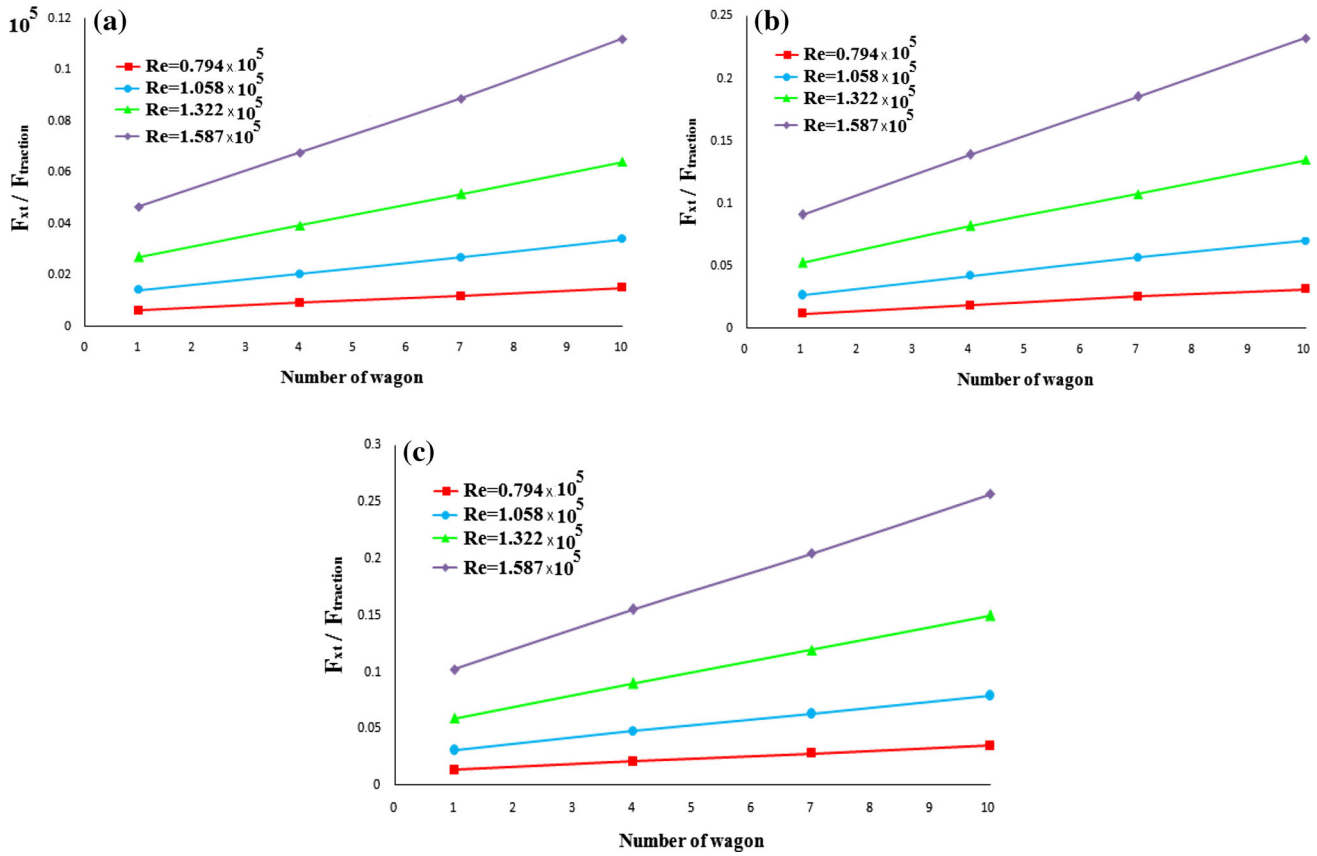

Fig. 15 Ratio of the total longitudinal force to the traction force for the configuration of the locomotive with one, four, seven, and ten wagons, at **a** $\alpha = 0°$, **b** $\alpha = 15°$, **c** $\alpha = 30°$

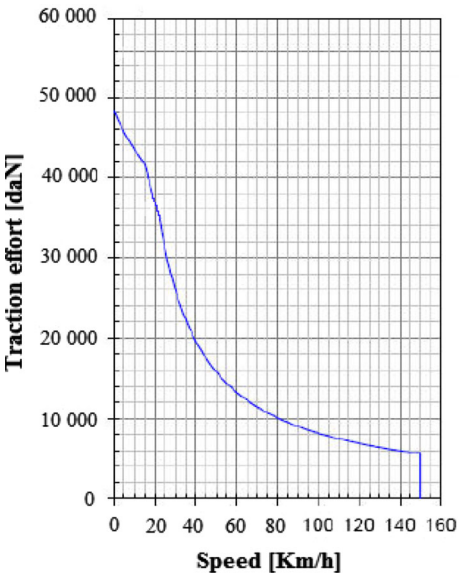

Fig. 16 Locomotive traction force for different train speeds

number 1.587×10^5. The increase in this ratio is not noticeable from the yaw angle 15°–30°. The fuel consumption also increases by approximately 25 % from the yaw angle 0°–30° for ten wagons at the Reynolds number 1.587×10^5.

5 Conclusion

In this study, the effect of different yaw angles on the pressure coefficients, LFC and SFC, and the fuel consumption of a passenger train, consisting of a locomotive and several wagons behind it, have been experimentally and numerically studied, and the following results have been obtained:

- The points 1 and 3 which are located in the vicinity of locomotive stagnation region and the flow separation region have the maximum and minimum pressure coefficients, respectively. These values are obtained by about 0.45 and −0.95 through the experimental investigation and 0.54 and −0.61 through the numerical simulation at the Reynolds number 1.587×10^5 and the yaw angle 0°.
- Comparison of the numerical and experimental results verifies the numerical simulation method. The maximum error occurs at the point 3 located on the

locomotive's top surface, where the flow separation happens.

- The deviation of airflow direction from yaw angle 0° has a significant effect on the airflow pattern and pressure distribution around the train. Increase in yaw angle leads to an increase in the value of the train LFC and SFC. The value of the total LFC for the configuration of the locomotive along with ten wagons is 3.565 at the yaw angle 30°.
- Increase in the number of wagons and the yaw angle causes the train LFC and SFC to increase.
- According to the air pressure distribution around the train, the variation of the LFC and SFC in the middle wagons (except for the first two and last two wagons) is similar. The average value of the aerodynamic characteristics of theses wagons can be considered as the aerodynamic characteristic of this specific passenger wagon when it is placed in the middle of the train. The average LFC and SFC for Reynolds number 1.587×10^5 are 0.1 and 0.004 at the yaw angle 0°; 0.221 and 0.416 at the yaw angle 15°; and 0.239 and 1.251 at yaw angle 30°, respectively.
- The deviation of airflow direction from the yaw angle 0° has a significant effect on the train fuel consumption.

References

Adams LF (1975) Engineering measurements and instrumentation. The English University Press Ltd., London

Astakhov PN (1966) Railway consist travel resistance. Transport, Moscow, p 178

Baker CJ (2003) Some complex applications of the wind loading chain. J Wind Eng Ind Aerodyn 91:1791–1811

Baker CJ (2010) The flow around high speed trains. J Wind Eng Ind Aerodyn 98:277–298

Baker CJ, Jones J, Lopez-Calleja F, Munday J (2004) Measurements of the cross wind forces on trains. J Wind Eng Ind Aerodyn 92:547–563

Chiu TW, Squire LC (1992) An experimental study of the flow over a train in a crosswind at large yaw angles up to 90°. J Wind Eng Ind Aerodyn 45:47–74

Churkov NA (2007) Railway train aerodynamics. Zheldorizdat, Moscow, p 332

Copley JM (1987) The three-dimensional flow around railway trains. J Wind Eng Ind Aerodyn 26:21–52

Diedrichs B (2003) On computational fluid dynamics modeling of crosswind effects for high-speed rolling stock. IMechE 217(F):203–226

Durst F, Khier W, Breuer M (2000) Flow structure around trains under side wind conditions: a numerical study. Comput Fluids 29:179–195

Golovanevskiy VA, Vitaly V, Chmovzh VV, Girka YV (2012) On the optimal model configuration for aerodynamic modeling of open cargo railway train. J Wind Eng Ind Aerodyn 107–108:131–139

Hemidia HN (2006) Large-eddy simulation of the flow around simplified high-speed trains under side wind conditions. Licentiate thesis, Göteberg, Chalmers University of Technology

Hoerner FS (1965) Fluid-dynamic drag. Hoerner, Bricktown, NJ, p 455

Holmes S, Schroeder M, Toma E (2000) High-speed passenger and intercity train aerodynamic computer modeling. IMechE, Orlando

Hoppmann U, Koenig S, Tielkes T, Matschke G (2002) A short term strong wind prediction model for railway application: design and verification. J Wind Eng Ind Aerodyn 90:1127–1134

Jalili MM, Faghih AK, Jahanmehr M, Behafarin V (2011) Experimental analysis of container waste due to wind erosion from different freight wagons. IMechE, Denver

Motallebi Hasankola SS, Goshtasbi Rad E, Abouali O (2012) Experimental investigation of the airflow around supported and surface mounted low rise rural buildings. Iran J Sci Technol (IJST) Trans Mech Eng 36(M2):143–153

Muld TM, Efraimsson G, Henningson DS (2012) Flow structures around a high-speed train extracted using proper orthogonal decomposition and dynamic mode decomposition. Comput Fluids 57:87–97

Plewa T, Linde T, Weirs G (2005) Adaptive mesh refinement—theory and applications. Springer, Chicago, pp 58–351

Sanquer S, Barré C, Virel M, Cléon L (2004) Effect of cross winds on high-speed trains: development of a new experimental methodology. J Wind Eng Ind Aerodyn 92:535–545

Suzuki M, Tanemoto K, Maeda T (2003) Aerodynamic characteristics of train/vehicles under cross winds. J Wind Eng Ind Aerodyn 91:209–218

Vasović I, Maksimović M, Puharić M, Matić D, Linić S (2011) Structural analysis of aerodynamic brakes in high-speed trains. Sci Tech Rev 61(2):10–15

Wilcox DC (1994) Turbulent modeling for CFD, 2nd edn. DCW Industries, California, pp 73–411